Three-dimensional electron momentum density of aluminum by $(\gamma,e\gamma)$ spectroscopy

C. Metz, Th. Tschentscher,* and P. Suortti
European Synchrotron Radiation Facility (ESRF), Boîte Postale 220, F-38043 Grenoble, France

A. S. Kheifets and D. R. Lun
Atomic and Molecular Physics Laboratory, Research School of Physical Sciences and Engineering, The Australian National University, Canberra ACT 0200, Australia

T. Sattler and J. R. Schneider
Hamburger Synchrotronstrahlungslabor (HASYLAB) at Deutsches Elektronen-Synchrotron (DESY), Notkestrasse 85, D-22603 Hamburg, Germany

F. Bell
Sektion Physik, Universität München, Am Coulombwall 1, D-85748 Garching, Germany
(Received 22 October 1998)

We report on the measurement of the three-dimensional electron momentum density (EMD) of aluminum. 150 keV photons with an intensity of 2×10^{11} photons/s from a multipole wiggler of the European Synchrotron Radiation Facility have been scattered at a 100 nm thin self-supporting aluminum foil and measured in coincidence with their recoil electrons. To improve the agreement with a full potential linear muffin-tin orbital theory, electron correlation effects have been incorporated via the so-called Lam-Platzman correction [Phys. Rev. B **9**, 5122 (1974)]. A comparison with two-dimensional angular correlation of annihilation radiation has been made and demonstrates the strong influence of the positron wave function on the EMD. In analogy to these experiments, we used the first derivative of the EMD as an indication of the Fermi breaks. [S0163-1829(99)13115-1]

I. INTRODUCTION

The strong interest in the electronic structure of solids led to the development of a large variety of experimental methods for the study of energy dispersion and density of states both for occupied and unoccupied bands: photoemission spectroscopy,[1] inelastic x-ray scattering,[2] electron-loss spectroscopy,[3] x-ray-absorption spectroscopy,[4] to name but a few. In contrast, a few methods exist which measure directly wave-function-related quantities such as the real-space electron density (x-ray form factors) or momentum densities. To the latter belongs the two-dimensional angular correlation of annihilation radiation[5] (2D-ACAR) — which, strictly speaking, measures the electron-positron pair density $\rho^{2\gamma}(\mathbf{p})$,[6] see Sec. II — $(\gamma,e\gamma)$ and $(e,2e)$ spectroscopy.[7] $(\gamma,e\gamma)$ experiments are an extension of the conventional Compton scattering where the double differential cross section describing the energy and angular distribution of the scattered radiation is proportional to the so-called Compton profile, which is defined as a twofold integration over the electron momentum distribution (EMD). This integration results from the lack of information about the momentum distribution of the recoiling electrons. Since integration averages over large volumes in momentum space, detailed information about solid-state effects such as Fermi surfaces or electron correlations might become difficult to obtain. It is therefore desirable to measure the EMD directly by fixing the complete scattering kinematics: if the momenta of the primary and scattered photon in addition to that of the recoil electron are measured simultaneously, i.e., in coincidence, the momentum of the electron in its initial state can be determined in a unique way. The corresponding triple differential cross section is proportional to the EMD itself. (We mention that the 3D-EMD can also be obtained indirectly by noncoincident Compton scattering if a rather large number of directional Compton profiles is measured and finally reconstruction techniques based on Fourier transforms are employed.[8]) The main difficulty of a $(\gamma,e\gamma)$ coincidence experiment originates in the strong incoherent elastic scattering of the recoiling electron within the target which disturbs the determination of the recoil momentum by multiple scattering. Since the mean free path for elastic scattering of electrons with a recoil energy of 51 keV is only about 44 nm in aluminum, self-supporting targets are required which are as thin as possible. In $(e,2e)$ experiments the photon is replaced by an electron. Though the scattering cross section is orders of magnitude larger than in the photon case (Rutherford versus Klein-Nishina), these experiments suffer even more from multiple scattering, partly because now two electrons are involved and partly since, at least up to now, rather low recoil energies ($\sim$1 keV) are used in these experiments.[9]

In the discussion of the 3D-EMD of aluminum, emphasis is put on electron correlation effects. In general, theoretical EMDs are obtained from an effective single-particle Schrödinger equation where the band states are populated due to occupation numbers from the interaction-free jellium model. They are corrected by the Lam-Platzman scheme[10] for electron correlation. Recent high-resolution conventional Compton scattering experiments on Li (Refs. 8 and 11) and Be (Ref. 12) indicate even stronger electron correlation effects

than expected in the Lam-Platzman approach based on a homogeneous interacting electron gas.[13]

II. METHOD

If a photon with energy ω and momentum $\mathbf{k}$ is scattered at an electron with energy $\epsilon>0$ and momentum $\mathbf{p}$, energy and momentum conservation laws yield for these energies and momenta

$$\epsilon=\omega-\omega'-E', \tag{2.1a}$$

$$\mathbf{p}=\mathbf{k}'+\mathbf{p}'-\mathbf{k}, \tag{2.1b}$$

where $(\omega',\mathbf{k}')$ and $(E',\mathbf{p}')$ are the energies and momenta of the photon and electron after the interaction. Thus, if $\mathbf{k}$, $\mathbf{k}'$, and $\mathbf{p}'$ are known experimentally, $\mathbf{p}$ can be determined in a unique way. For the coincident detection of both the scattered photon with $(\omega',\mathbf{k}')$ and the recoil electron $(E',\mathbf{p}')$, the triple differential cross section

$$\frac{d^3\sigma}{d\omega' d\Omega_\gamma d\Omega_e}=\frac{\omega}{\omega'}p'\left(\frac{d\sigma}{d\Omega_\gamma}\right)_{\mathrm{KN}}\rho(\mathbf{p}) \tag{2.2}$$

holds,[14] where $\rho(\mathbf{p})$ is the EMD and $(d\sigma/d\Omega_\gamma)_{\mathrm{KN}}$ is the Klein-Nishina cross section for linearly polarized photons. The validity of the so-called impulse approximation is assumed. We mention that the term ''impulse approximation'' has a different meaning for the triple and the double differential cross section, respectively. Whereas for the triple differential cross section the final electron states are approximated by plane waves, one assumes in addition plane waves also for the initial state in case of the double differential cross section. The momentum distribution of the plane waves is that of the EMD of the initial state. The possibility of this approximation (the so-called ''potential cancellation'') relies strongly on the completeness relation for the electron states[15,16] which cannot be used in the case of the triple differential cross section. Eisenberger and Platzman[15] have evaluated the nonrelativistic photon scattering matrix element within the first Born approximation with correct eigenstates of the unperturbed Hamiltonian for the initial and final electron states. This matrix element can be calculated analytically. One can easily show that for a given momentum transfer the impulse approximation works better in the case of the double than of the triple differential cross section. Whereas in the former case the momentum transfer can even be of the order of the initial electron momentum, it should be larger at least by an order of magnitude in the latter case in order to obtain a reasonable approximation. It was demonstrated by Surić[17] that this statement holds also for the relativistic external field S-matrix element within the independent-particle approximation.

Usually, the EMD for crystalline solids is obtained from a band-structure calculation. Due to translational invariance the corresponding wave functions are Bloch waves

$$\phi_{\mathbf{k},i}(\mathbf{r})=u_{\mathbf{k},i}(\mathbf{r})e^{i\mathbf{k}\cdot\mathbf{r}}, \tag{2.3}$$

where the crystal momentum $\mathbf{k}$ is restricted to the first Brillouin zone and i is the band index. From the lattice periodicity of $u_{\mathbf{k},i}(\mathbf{r})$ follows

$$u_{\mathbf{k},i}(\mathbf{r})=\sum_{\mathbf{g}} A_{\mathbf{g},i}(\mathbf{k})e^{i\mathbf{g}\cdot\mathbf{r}}. \tag{2.4}$$

Evaluating the Fourier transform $\phi_{\mathbf{k},i}(\mathbf{p})$ of Eq. (2.3) yields the EMD $\rho(\mathbf{p})$,

$$\rho(\mathbf{p})=2\sum_{\mathbf{k},\mathbf{g},i} n_i(\mathbf{k})|\phi_{\mathbf{k},i}(\mathbf{p})|^2$$

$$=2\sum_{\mathbf{k},\mathbf{g},i} n_i(\mathbf{k})|A_{\mathbf{g},i}(\mathbf{k})|^2\delta(\mathbf{p}-\mathbf{k}-\mathbf{g}). \tag{2.5}$$

$n_i(\mathbf{k})$ are the occupation number densities. Within the independent-particle model they are equal to unity for momenta smaller than the Fermi momentum and zero above. This holds for the reduced zone scheme. Nondiagonal elements n_{ij} of the occupation number density due to electron-electron interaction (equivalent to configuration interaction in Hartree-Fock theory) are believed to be negligible, at least when the nearly-free-electron approximation is applicable.[18] For comparison we mention that the corresponding expression in the case of ACAR yields for the electron-positron pair density[19]

$$\rho^{2\gamma}(\mathbf{p})=2\sum_{\mathbf{k},\mathbf{g},i} n_i(\mathbf{k})|A^{+-}_{\mathbf{g},i}(\mathbf{k})|^2\delta(\mathbf{p}-\mathbf{k}-\mathbf{g}), \tag{2.6}$$

where the Fourier components of the corresponding electron-positron Bloch state are given by

$$A^{+-}_{\mathbf{g},i}(\mathbf{k})=\sum_{\mathbf{g}'} A^{+}_{\mathbf{g}'}(0)A^{-}_{\mathbf{g}-\mathbf{g}',i}(\mathbf{k}), \tag{2.7}$$

A^- and A^+ being the separate Fourier components of the electron and positron wave function, respectively. It is readily seen that, except for a positron wave function $u^+_0(\mathbf{r})=\mathrm{const}$, i.e., $A^+_{\mathbf{g}}=\delta(\mathbf{g})$, the densities of Eqs. (2.5) and (2.6) are different.

III. EXPERIMENT

The experiment was performed at the high-energy x-ray scattering beamline ID15A of the ESRF.[20] An asymmetric wiggler with seven periods and strong poles of 1.8 T was used with a critical energy of 44.1 keV at a gap of 20.3 mm. The white beam was monochromatized by a (220) bent Si crystal in Laue geometry [$\Delta\omega=0.74$ keV full width at half maximum (FWHM)]. The photon beam entered an evacuated target chamber (10^{-3} Pa) with an externally mounted intrinsic Ge diode (energy resolution 0.4 keV FWHM at 100 keV) at a scattering angle of $\theta=140°$. The electrons were measured by means of a two-dimensional position sensitive detector (PSD) which consisted of 16×16 individual photodiodes (Fig. 1). The experimental setup will be described in more detail in a forthcoming publication.[21] The center of the array was placed in the direction of the momentum transfer vector $\mathbf{q}_0=\mathbf{k}-\mathbf{k}'_0$, where $\mathbf{k}'_0$ is the momentum of photons scattered at electrons at rest. Since both the energy resolution of the photon and electron detector are large compared to the binding energy ϵ of the valence electrons — which dominate the EMD — we measured the direction of $\mathbf{p}'$, but the modulus was obtained from the energy conservation law of Eq.

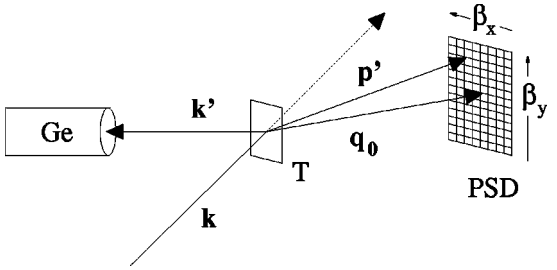

FIG. 1. Experimental setup: Ge, Ge diode; *T*, target; PSD, position-sensitive electron detector.

(2.1): $|p'|=[(\omega-\omega'+1-\epsilon)^2-1]^{1/2}$, neglecting ϵ, which is of the order of tens of eV at most compared to $\omega=150$ keV and $\omega'\cong\omega_0'=99$ keV. For the same reason the influence of the work function on the electron energy is disregarded. From kinematics one obtains[22] for the Cartesian components of the initial electron momentum **p**

$$p_x=q_0\beta_x+\omega\sin(\theta)\Delta\omega'/q_0, \tag{3.1a}$$

$$p_y=q_0\beta_y, \tag{3.1b}$$

$$p_z=-\omega\Delta\omega'/(q_0\omega_0'), \tag{3.1c}$$

where β_x and β_y are the angular deviations of $\mathbf{p}'$ from $\mathbf{q}_0$ (see Fig. 1) and $\Delta\omega'=\omega'-\omega_0'$ with

$$\omega_0'=\frac{\omega}{1+\omega[1-\cos(\theta)]} \tag{3.2}$$

the energy of photons scattered at electrons at rest (we use natural units with $\hbar=m=c=1$). For a primary photon energy $\omega=150$ keV and a scattered energy $\omega_0'=99$ keV the momentum transfer $q_0=63$ a.u. is very much larger than the initial momentum **p** which is essential for the validity of the impulse approximation.[15] Detailed Monte Carlo (MC) simulations of the momentum resolution of the $(\gamma,e\gamma)$ spectrometer included the correlated scattering due to the triple differential cross section of Eq. (2.2), solid angle and energy resolution of the Ge diode, energy broadening of the primary beam, and the extension of the beam spot at the target. The variance vector for the momentum errors in the three Cartesian directions obtained by these MC calculations was $\sigma_p=(0.18,0.43,0.20)$ a.u. Emission patterns of the recoiling electrons which were broadened due to this variance vector were recorded by the 2D electron detector with a granularity of about 0.14 a.u in p_x and 0.28 a.u. in p_y. Thus, the variance both in the p_x and p_y direction extended over approximately 1 pixel. The time resolution of the coincidence was about 200 ns, considerably longer than the bunch distance of 3 ns in the so-called 2/3 fill mode of the ESRF. Time correlation spectra showed very little chance coincidences which nevertheless were taken into account. The overall coincidence rate due to a primary beam of about 2×10^{11} photons/s was about 1.5 Hz at an average beam current of 100 mA. A total of 5.4×10^5 coincidence events were accumulated.

The target was a 100 nm thin self-supporting polycrystalline Al foil with a diameter of 12 mm [the beam spot was 1.2 mm (horizontal)$\times$4.0 mm (vertical)]. Targets prepared by aluminum evaporation on a thin Betaine film

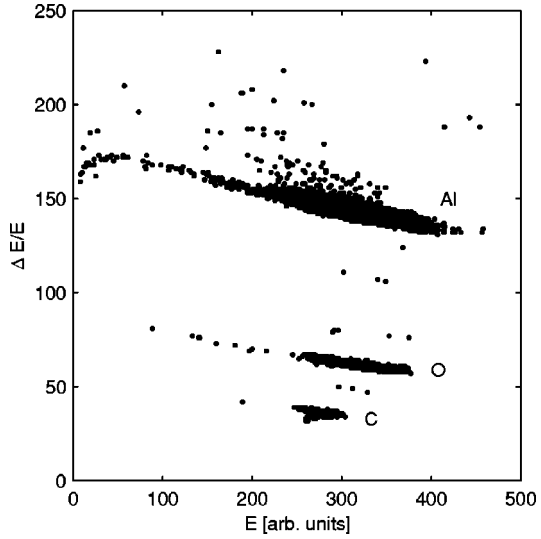

FIG. 2. Scatter plot of the ERDA measurement: relative energy loss $\Delta E/E$ against recoil energy E. The contributions from Al, O, and C are indicated.

($C_5H_{11}NO_2\cdot H_2O$) which had a fine crystallinelike structure that acted as a replica for the Al film and guaranteed some mechanical stability. Finally, the Betaine film was dissolved in water and the Al foil was put free standing onto frames. It is well known that aluminum metal readily oxidizes at its surface. Though passivation of aluminum leads to a saturated oxide layer with thicknesses of about 1.5–2 nm only,[4,23,24] we have investigated our foils quantitatively by elastic recoil detection analysis (ERDA) of fast heavy ions at the Munich heavy ion accelerator. A 210 MeV ^{127}I beam hits the Al film while a 2D-ionization chamber at a large scattering angle detects recoil ions emitted from the target.[25] The energy loss ΔE of the recoils ions, dominated by electronic processes, is analyzed by an energy dispersive detector. Since $\Delta E\sim Z^2$, Z being the nuclear charge of the recoil ions (Bethe-Bloch regime), and the scattering cross section, in this case the Rutherford cross section, is well known, the ERDA method is able to determine quantitatively the composition of the target. Figure 2 shows the relative energy loss $\Delta E/E$ of the recoil ions as a function of the recoil energy E. There is a distribution of recoil energies since the recoil atoms are distributed within the target. Figure 2 holds for a 100-nm thin Al target. Very clearly the signals from Al, O, and C can be seen. The intensities correspond to a contamination of 6.3 at.% oxygen and 0.6 at.% carbon. Figure 3 shows the intensity of oxygen recoil ions as a function of their energy E. There are two prominent contributions, indicating that oxygen is deposited on the front and backside of the foils (and not in the interior). With the assumption that two Al_2O_3 layers have been formed, we calculate a thickness of 1.0 nm for each of them. While this thickness coincides with measurements of aluminum passivation,[4,23,24] it is in contrast to results by Sakurai *et al.*,[26] who estimated by electron spectroscopy for chemical analysis (ESCA) an oxide layer of 20 nm on an 85-nm thin aluminum foil. The authors used this relatively strong contribution of Al_2O_3 to explain that their $(\gamma,e\gamma)$ experiment showed a remarkably broader EMD than expected from pure aluminum.

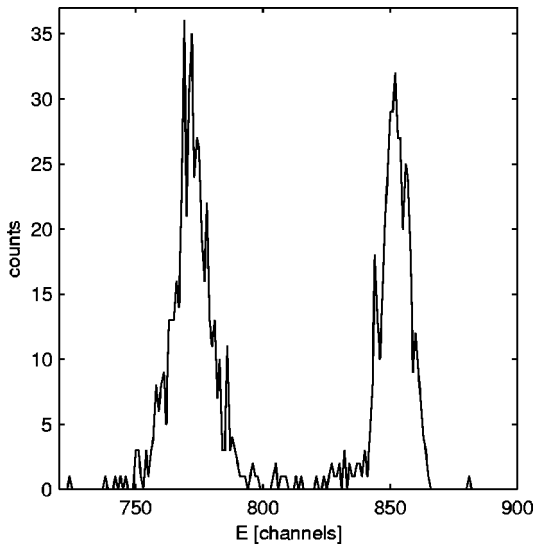

FIG. 3. The intensity of scattered oxygen recoil ions as a function of their energy E. Signals from both sides of the Al foil can be identified.

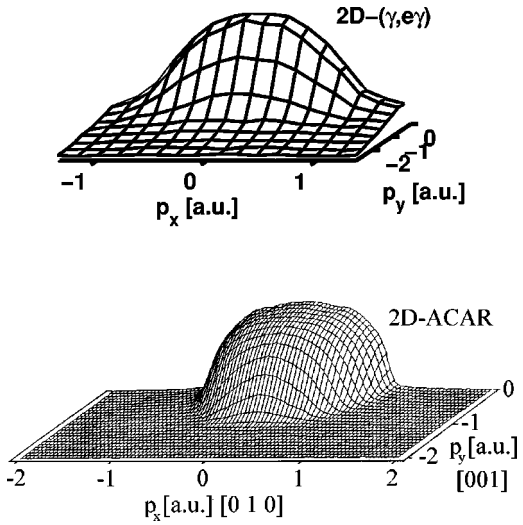

FIG. 4. 2D angular correlation plots for $(\gamma,e\gamma)$ and ACAR measurements (Ref. 31).

IV. EXPERIMENTAL RESULTS AND DISCUSSION

A comparison between the experimental EMD and theoretical results from band-structure calculations has been made by normalizing both to the same integral value within an integration volume $p_x=\pm 1.4$ a.u., $p_y=\pm 2.5$ a.u., $p_z=\pm 6$ a.u., which is given primarily by the finite extension of the electron detector. In essence, the Fourier components $A_{\mathbf{g},i}(\mathbf{k})$ of Eq. (2.4) have been calculated by the linear muffin-tin orbital method either in the atomic sphere[27] (ASA-LMTO) or the full potential approximation (FP-LMTO).[28] In the ASA-LMTO a unit cell of the crystal is substituted by a number of overlapping atomic spheres with no room left for the interstitial region. The electron potential is assumed to be spherically symmetric inside the spheres. In the FP-LMTO a number of nonoverlapping muffin-tin spheres is introduced, the potential is expanded in spherical harmonics inside the spheres, and is Fourier transformed in the interstitial region. This treatment of the interstitial region provides superior accuracy at the price of increasing computation time.

LMTO is one of many computational schemes derived within the general density-functional philosophy. A detailed comparison of ASA-LMTO with $(e,2e)$ experiments is given in Refs. 9 and 29 with additional attention to photoemission spectroscopy. The occupation number density $n_i(\mathbf{k})$ for both approximations is that of the noninteracting electron gas. For comparison with experimental data, a MC code was established which, in addition to the experimental finite resolutions of Sec. III, incorporated the theoretical EMD and the elastic multiple scattering of the emerging electrons within the target (due to the energy resolution of about 2.8 keV of the electron detector, inelastic multiple scattering mainly due to plasmon losses of about some tens of eV has been disregarded). The treatment of multiple scattering follows closely that of Salvat *et al.*,[30] using the elastic cross sections of Wigner-Seitz atoms in a solid.

2D or 3D EMDs of aluminum have been measured in the past both by ACAR (Refs. 5 and 31) and by the $(e,2e)$ technique.[9,29,32] For comparison with 2D-ACAR data we have evaluated from our results the angular correlation density

$$\rho^{2D}(p_x,p_y)=\int \rho(p_x,p_y,p_z)dp_z, \tag{4.1}$$

which is plotted in Fig. 4 together with 2D-ACAR from Ref. 31. It is readily seen that in the ACAR data the EMD is cut off at $p_x=p_y\cong 1$ a.u. due to the positron wave function being repelled from the ion core. Recent calculations by Alatalo *et al.*[33] show a drastic reduction of the positron wave function in aluminum for distances below 2 a.u. in real space. Nothing like that happens in the $(\gamma,e\gamma)$ experiment, which shows appreciable intensity beyond 1 a.u. due to the core states. Figure 5 shows the EMD at $p_x=p_y=0$ as a function of p_z in comparison with the FP-LMTO theory including the Lam-Platzman (LP) correction, see below, and the contribution from the Al_2O_3 layer on both surfaces, see Sec.

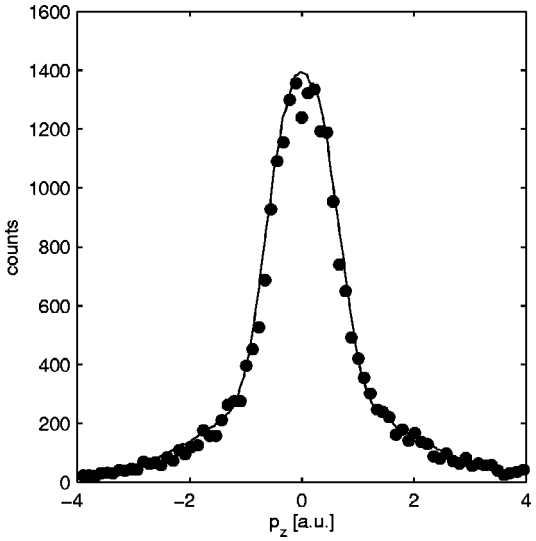

FIG. 5. The experimental EMD $\rho(0,0,p_z)$ (dots) compared to theory (solid line) including the instrument resolution. From the global normalization one has $\chi_L^2=3.9$.

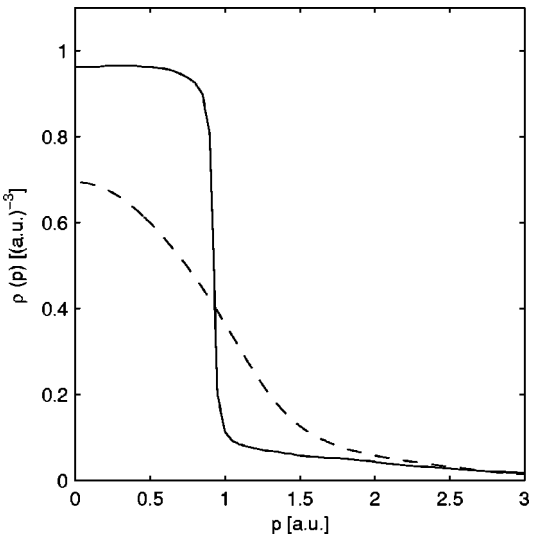

FIG. 6. The spherically averaged theoretical EMDs of Al (solid curve) and Al_2O_3 (broken curve) normalized to the same number of electrons.

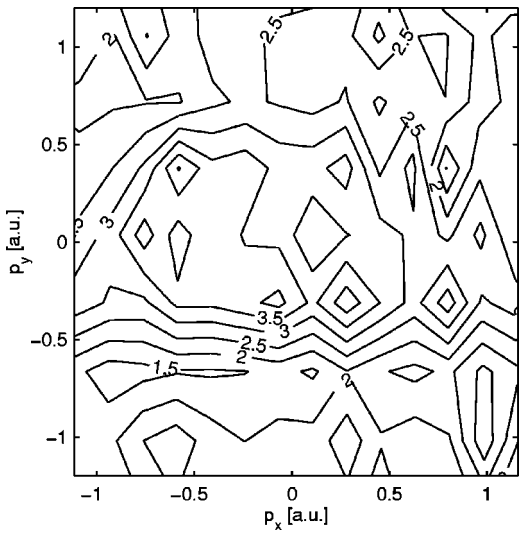

FIG. 7. Isodensity plot of the likelihood χ_L^2 in the (p_x,p_y) plane, indicating that the agreement between experiment and theory is comparable to that of Fig. 5 for the whole (p_x,p_y) plane.

III. For the α-Al_2O_3 EMD (corundum structure) we used an ASA-LMTO calculation with von Barth and Hedin parametrization for the exchange-correlation potential.[34] Figure 6 shows the spherically averaged theoretical EMDs for aluminum and α-Al_2O_3 normalized to the same number of electrons. One observes immediately the sharp Fermi break due to unfilled bands in the metal aluminum in contrast to the smooth EMD of the ionic insulator Al_2O_3. In all the EMD figures shown in this work the contribution due to α-Al_2O_3 has been added. The likelihood χ_L^2,

$$\chi_L^2=(2/n)\sum_{i=1}^{n}\left[y_i-x_i+x_i\ln(x_i/y_i)\right], \tag{4.2}$$

where y_i is the theoretical prediction and x_i is the experimental value in the ith bin,[35] amounts for the experimental results of Fig. 5 to $\chi_L^2=3.9$ in the range -6 a.u.$\leqslant p_z\leqslant 6$ a.u. We would like to stress that this value was not obtained by minimizing with respect to the theoretical curve of Fig. 5 but was calculated from the global normalization. Figure 7 demonstrates that the quality of agreement is roughly the same if the comparison between theory and experiment is extended from $p_x=p_y=0$ to the whole (p_x,p_y) plane.

EMDs obtained from the pseudo-wave-functions of density-functional theory (''Kohn-Sham equations'') are not correct due to exchange-correlation effects.[36] Their accuracy can be improved by adding the Lam-Platzman correction[10] $\Delta\rho_{\rm LP}(p)$ to the EMD,

$$\Delta\rho_{\rm LP}(p)=\delta E^{\rm XC}/\delta\epsilon_p\cong\int_\Omega\rho(\mathbf{r})3\Delta N/(4\pi p_F^3)d^3\mathbf{r}, \tag{4.3}$$

where the correction term is given by the derivative of the total exchange-correlation energy $E^{\rm XC}$ with respect to the individual electron energy ϵ_p, $\rho(\mathbf{r})$ is the electron density, and $\Delta N=N^{\rm ie}(p)-N^f(p)$. $N^{\rm ie}$ and N^f are the occupation number densities of the homogeneous interacting and the free electron gas (jellium), respectively. Connection with Eq. (2.5) is made by recognizing that

$$N(\mathbf{p})=\sum_i n_i(\mathbf{p}) \tag{4.4}$$

in the repeated zone scheme. The integration in Eq. (4.3) extends over the volume Ω of the Wigner-Seitz sphere (Al: $\Omega=110$ a.u.^{3}).

In the following we will focus on the question of whether our experimental data indicate the significance of the Lam-Platzman correlation correction term. To do so, we have calculated $\Delta\rho(p)$ with a parametrization of ΔN due to Schülke *et al.*,[8]

$$\Delta N=\begin{cases}-a-\frac{1}{2}(1-a-Z_{p_F})\left(\dfrac{p}{p_F}\right)^8 & \text{for } p\leqslant p_F\\[2ex] \frac{1}{2}(1-a-Z_{p_F})\left(\dfrac{p_F}{p}\right)^8 & \text{for } p\geqslant p_F\end{cases} \tag{4.5}$$

with $a=9(1-Z_{p_F})/64$. It is obvious that for an interacting electron gas with a renormalization constant $Z_{p_F}<1$, also states above the Fermi momentum p_F become occupied.[13] According to Lundqvist[37] the single-particle hole couples to the plasmon (yielding a quasiparticle called plasmaron) with a lifetime broadening near the Fermi momentum which results in the $(p/p_F)^{-8}$ tails of Eq. (4.5). The spectral weight of this mode is given by Z_{p_F}. To obtain $\Delta\rho_{\rm LP}(p)$ we used the FP-LMTO electron density $\rho(\mathbf{r})$ since in the spirit of the local-density approximation both p_F and Z_{p_F} become functions of r_s, i.e., of the electron density $\rho(\mathbf{r})$: $p_F=(9\pi/4)^{1/3}r_s^{-1}$. For $Z_{p_F}(r_s)$ we used Eq. (36a) of Ref. 38. For comparison we have also calculated the correction $\Delta\rho_{\rm LP}^v$ for the constant valence electron density $\rho_v=3/\Omega$ in aluminum. For this case Eq. (4.3) yields $\Delta\rho_{\rm LP}^v=\Delta N\Omega/(4\pi^3)$ with the Fermi momentum $p_F=0.93$ a.u. and a renormalization

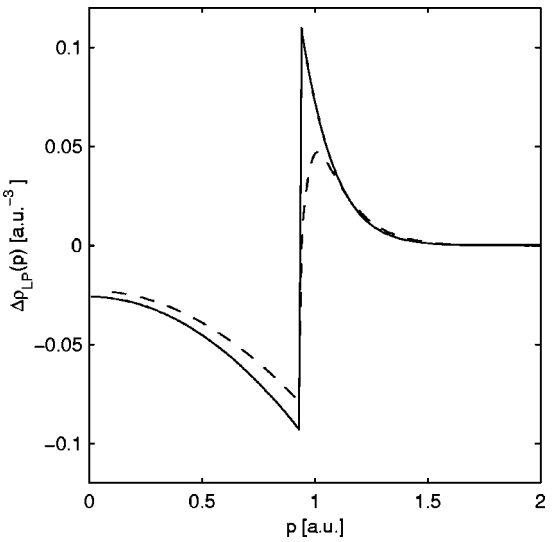

FIG. 8. $\Delta\rho^{v}_{\mathrm{LP}}$ (solid) and $\Delta\rho_{\mathrm{LP}}$ (dashed) for the renormalization constant of Ref. 38.

constant $Z_{p_F}=0.763$ which corresponds to $r_s=[3/(4\pi\rho_v)]^{1/3}=2.1$. This value of Z_{p_F} has been calculated by Hedin[39] within the so-called G_0W_0 approximation of the self-energy operator. Figure 8 shows both $\Delta\rho^{v}_{\mathrm{LP}}$ and $\Delta\rho_{\mathrm{LP}}$ as a function of the momentum p. A comparison of both corrections demonstrates that the Lam-Platzman correction is dominated by the valence electrons: with increasing electron density $\rho(\mathbf{r})\Delta N$ tends to zero: a large density means also a large kinetic energy of the electrons ($\propto r_s^{-2}$) which outbalances the increased electrostatic interaction between the electrons ($\propto r_s^{-1}$), i.e., they behave more like a free-electron gas.

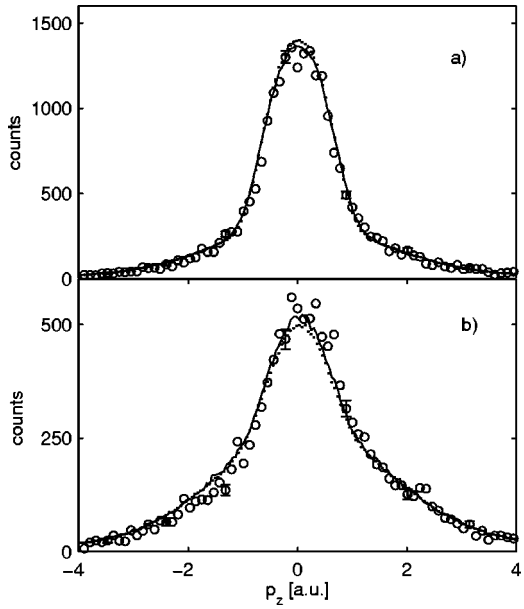

FIG. 9. A comparison between the experimental EMD (error bars) and the LMTO calculation with (solid) and without (dotted) the Lam-Platzman (LP) correction $\Delta\rho_{\mathrm{LP}}$. (a) holds for $p_x=0.1$ a.u., $p_y=0.2$ a.u.; (b) for $p_x=1.1$ a.u., $p_y=0.2$ a.u. The likelihood amounts to $\chi_L=3.5$ (with LP) and $\chi_L=3.9$ (without LP) for (a) and $\chi_L=5.8$ (with LP) and $\chi_L=6.6$ (without LP) for (b). Representative error bars due to statistical uncertainties are indicated.

Quantitatively the correction $\Delta\rho_{\mathrm{LP}}$ amounts to a subtraction of 3% from $\rho(0)$ at $\mathbf{p}=\mathbf{0}$. Clearly, momentum density is transferred from low momenta to higher ones. Figure 9 shows experimental EMDs together with curves from the FP-LMTO theory including (solid line) and without (dotted line) the Lam-Platzman correction. (Treated by the MC simulation, the difference of both Lam-Platzman corrections of Fig. 8 becomes considerably less than the experimental uncertainty. Actually we used $\Delta\rho^{v}_{\mathrm{LP}}$ in the following.) Figure 9(a) holds for $p_x=0.1$ a.u., $p_y=0.2$ a.u., Fig. 9(b) for $p_x=1.1$ a.u., $p_y=0.2$ a.u. The correction is most pronounced at $p_z=0$, which corresponds to electron momenta $p=0.2$ a.u. [Fig. 9(a)] and $p=1.1$ a.u. [Fig. 9(b)], respectively. From the different sign of the correction it becomes evident that momentum density is transferred to momenta larger than the Fermi momentum $p_F=0.93$ a.u. The likelihood changes from $\chi_L=3.9$ to $\chi_L=3.5$ if the LP correction is included [Fig. 9(a)] and from $\chi_L=6.6$ to $\chi_L=5.8$ for Fig. 9(b). These values hold for the range -1.5 a.u.$\leqslant p_z \leqslant 1.5$ a.u., though, of course, the fit of theory to experiment results from the global normalization. It is evident that the LP correction improves the agreement between theory and experiment in the region of the valence electrons. Comparing Figs. 9(a) and 9(b), it is also evident that the shape of both EMD cuts is remarkably different: whereas in Fig. 9(a) a pronounced change of the slope can be seen at $p_z\cong 0.9$ a.u., which is a reminiscence of the Fermi break, Fig. 9(b) represents the continuous decrease of the EMD due to core states. The LMTO calculation has been done for the valence electrons only, i.e., lacking core orthogonalization [18,40] (the core momentum density was calculated from the Roothaan-Hartree-Fock wave functions of Bunge *et al.*[41]). Since the lattice potential has a very weak influence on the valence electrons, we assume that the orthogonalization effect in aluminum is just as small as in sodium, where it was demonstrated by Lundqvist and Lydén[18] that the generation of high momentum components due to orthogonalization is negligible compared to electron correlation effects. We remark that a recent fully self-consistent *GW* self-energy calculation,[42] where the self-consistent Green's function G is obtained from Dyson's equation, yields for the renormalization constant $Z_{p_F}=0.846$ at $r_s=2$, a value which would slightly reduce the agreement of Fig. 9. For a recent review of the *GW* method, see the article of Aryasetiawan and Gunnarsson.[43]

If all the events for a constant p_z value are summed up, we obtain what is called a coincident Compton profile J_{coinc}, a procedure which increases statistics considerably. Due to the limited range of our experiment in the p_x and p_y direction this coincident Compton profile is not identical to a noncoincident one, but it has the advantage of increasing statistics within the region of the valence electrons while the contribution of core states is reduced. In addition, the trigger condition provides photon spectra free of any background radiation. In Fig. 10 we compare J_{coinc} with theory: the dash-dotted curve is due to ASA-LMTO, the dotted curve results from FP-LMTO, whereas the solid curve incorporates in addition to FP-LMTO the LP correction. Clearly, the agreement with experiment is progressively improved. This is also demonstrated on a larger scale in Fig. 11, where the difference $\Delta J_{\mathrm{coinc}}$, i.e., experiment minus theory, is plotted as a

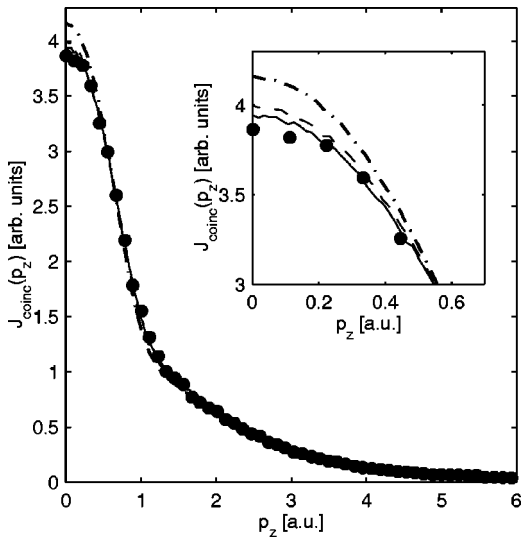

FIG. 10. The coincident Compton profile J_{coinc}. Dots: experiment (the dot size represents the statistical uncertainty); dash-dotted: ASA-LMTO approximation; dashed: FP-LMTO approximation; solid: FP-LMTO approximation including the LP correction. The inset shows the curves at low momenta on an enlarged scale.

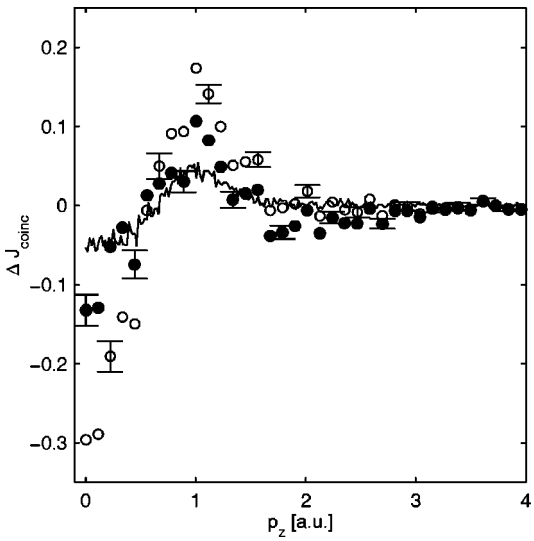

FIG. 11. The difference $\Delta J_{\mathrm{coinc}}$ between experiment and theory (open circles: ASA-LMTO approximation; dots: FP-LMTO approximation). The solid curve represents the LP correction.

function of p_z. Open circles represent ASA-LMTO, dots FP-LMTO, and the solid line the LP correction (the ''noise'' on this curve results from the MC simulation). It is evident that the FP-LMTO is superior to ASA-LMTO in describing the experiment by transferring intensity from low momenta to higher ones. The LP correction further improves the agreement between experiment and theory, though it is not perfect. We mention that the band structures for the occupied states from both theories are very similar. Differences — including those of bandwidth and gaps — are at the mRy level and would thus be hardly detectable on an absolute scale, e.g., by angle-resolved photoemission experiments.[1] Though also the EMD's of both theories differ by a few percent only, this effect can be detected by Compton scattering unambiguously as shown by Figs. 10 and 11. We also remark that the LP correction is insensitive to the special representation of the occupation number density N^{ie} of Eq. (4.5). Using the slightly different expression of Farid *et al.*[38] does not change the LP correction of Fig. 11.

The influence of electron correlation has also been investigated in earlier Compton profile measurements by Cardwell and Cooper.[44,45] An improvement in the agreement between experiment and calculations based on density-functional theory was observed. High-resolution Compton profile measurements by Shiotani *et al.*[46] showed a deviation of the experiment from the inverted parabola of the free-electron gas around p_F but no quantitative analysis according to the Lam-Platzman correction was made. Finally we want to comment on the influence of multiple electron scattering. In principle, one could argue that multiple scattering broadens the EMD, thus transferring intensity from low to higher momenta, which could mimic correlation effects. That this in fact does not happen relies on the very different influence of multiple scattering on the three Cartesian components of the momentum **p**. Since it changes primarily the emission angles β_x and β_y of the emerging electrons, it is readily seen from the kinematics of Eq. (3.1) that only the components p_x and p_y are dominantly influenced by multiple scattering. The difference of the coincident p_z-dependent photon spectra for an arbitrary thin and an infinitely thick target — with respect to electron multiple scattering — is that of a cut through the 3D EMD and an ordinary Compton profile. Compared to a completely flat distribution in the p_x and p_y direction for the latter case, this is a rather small change. This is also substantiated by our MC code: enlarging the foil thickness by 50% — actually the thickness can be determined within 5% — does not change the shape of the theoretical curves in Fig. 9 remarkably. It should be noted that these are p_z-dependent cuts through the EMD. Thus we conclude that multiple scattering cannot simulate correlation effects.

As stated in the Introduction, ACAR measures not the EMD but the positron-electron pair correlation density. Though the positron strongly polarizes the electron gas, the position of the Fermi breaks remains unchanged.[6] It is for

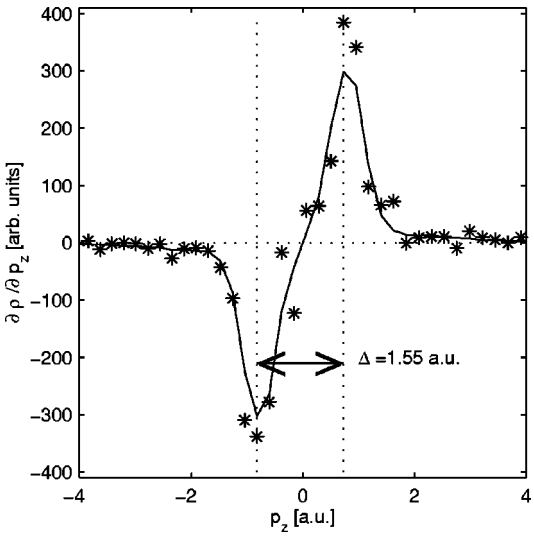

FIG. 12. First derivative $\partial\rho/\partial p_z$ of the EMD (stars) compared to theory (solid line). The data hold for $p_x = 0.1$ a.u., $p_y = 0$ and the distance between the extrema amounts to $\Delta = 1.55$ a.u.

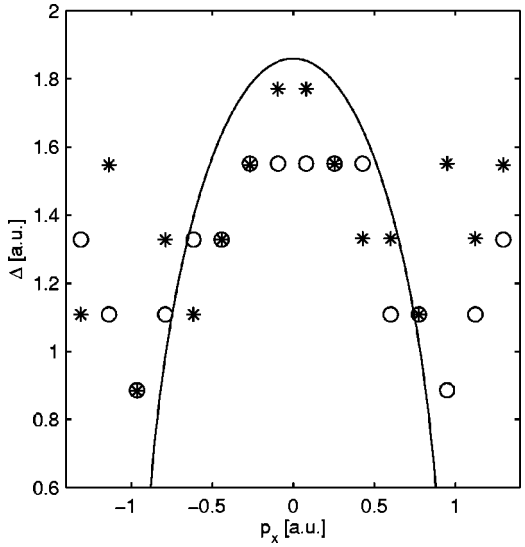

FIG. 13. The distance Δ between the extrema (see Fig. 12) as a function of p_x for $p_y=0$. Stars are from the experiment, open dots hold for theory. The solid line represents the free-electron-gas model without any folding with resolution.

this reason that the ACAR measurements have widely been used for the evaluation of the Fermi surface topology (fermiology) mostly by differentiating the angular correlation data and looking for the extrema. Though our data have significantly fewer statistics and lower resolution, we will briefly discuss the outcome of such a procedure for $(\gamma,e\gamma)$ measurements. Figure 12 shows $\partial\rho/\partial p_z$ as a function of p_z for $p_x=0.1$ a.u, $p_y=0$. Black stars are the experimental derivatives, whereas the solid line represents the LMTO theory including LP correction. For $p_x=0.1$ a.u., $p_y=0$ the distance Δ between the experimental extrema amounts to $\Delta=1.55$ a.u. In Fig. 13 the distance Δ is plotted as a function of p_x for $p_y=0$. Stars are taken from the experimental derivatives, open dots from the corresponding theory. For an arbitrary good resolution all points should be represented by the nearly-free-electron result (solid line) within the range $-p_F \leqslant p_x \leqslant p_F$. Finite resolution causes that approximately 80% of the extreme value at the descending part of the derivate yields the correct Fermi surface, an experience also made by ACAR measurements.[47] For $|p_x|>p_F$ the distance Δ increases again due to the influence of core states. The slightly asymmetric behavior of the theoretical points in Fig. 13 with respect to p_x results primarily from the kinetics of Eq. (3.1a): while multiple scattering is symmetric in β_x its influence on $\Delta\omega'$ is negligible, which means an offset of the symmetry. We conclude this section with some general remarks about the possibilities of the $(\gamma,e\gamma)$ technique. The strong influence of electron multiple scattering restricts the method to thin foils and low Z material, nevertheless we emphasize that investigations of Cu_xNi_{1-x} alloys have been successfully made.[48] Since epitaxially grown films are available, measurements with single crystals are possible. On the experimental side a multiple pixel γ detector could easily improve the count rate by an order of magnitude.

V. SUMMARY

We have measured the 3D EMD of thin polycrystalline Al foils and compared it with a LMTO calculation, which is based on the density-functional idea. The agreement between experiment and theory could essentially be improved by taking into account electron correlation. Though theory incorporated the exchange-correlation potential with the parametrization of van Barth and Hedin,[49] a further important effect of electron-electron interaction is a change of the occupation number density from that of the free-electron gas. The interaction pushes a part of the occupied states below the Fermi momentum p_F to momenta above p_F. Within the spirit of the local-density approximation (LDA) this change of occupation number density can be accounted for by the so-called Lam-Platzman correction.[10] Applied to the EMD of aluminum, the agreement for momenta both $p<p_F$ and $p>p_F$ considerably improved. The renormalization constant $Z_{p_F}=0.76$ is that of the interacting electron gas at $r_s=2.1$. In spite of its great simplicity, this correction seems to represent electron correlation in momentum densities quite correctly: recent calculations[50] of the Compton profile of silicon by *ab initio* nonlocal pseudopotential variational quantum Monte Carlo techniques, where correlation has been included into the many-body wave function via a Jastrow factor, demonstrate that correlation correction to the LDA Compton profile is well reproduced by the Lam-Platzman term. 2D angular correlation plots are compared to 2D ACAR and show the strong influence of the positron wave function. Despite the rather poor statistics and low resolution, we have shown that the extrema of the first derivative of the EMD (which corresponds to the second derivative of a Compton profile) give an indication of the Fermi momenta, which do agree well with respect to theoretical calculations. We also emphasize that complex many-body effects such as positron-induced polarization, which results in an enhancement of the electron density,[6,5] are naturally absent in the $(\gamma,e\gamma)$ reaction.

ACKNOWLEDGMENTS

The authors thank Dr. H. J. Maier and D. Frischke from the Munich Target Lab for the preparation of the aluminum foils, and Dr. W. Assmann from the Munich Heavy Accelerator Group for the ERDA measurements. A.S.K. acknowledges support from the Australian Research Council, and Ch.M. acknowledges a grant from the ESRF. This work was supported by the Bundesministerium für Bildung, Wissenschaft, Forschung und Technologie, Contract Nos. 05 5WMAAI and 05 ST8HRA.

*Present address: HASYLAB (DESY), Hamburg, Germany.

[1] H. Levinson, F. Greuter, and E. Plummer, Phys. Rev. B **27**, 727 (1983).

[2] W. Schülke, H. Schulte-Schrepping, and J. Schmitz, Phys. Rev. B **47**, 12 426 (1993).

[3] J. Fink, in *Unoccupied Electronic States*, edited by J. Fuggle and

J. Inglesfield (Springer, Berlin, 1992), Vol. 69.
[4] I. Batra and L. Kleinman, J. Electron Spectrosc. Relat. Phenom. **33**, 175 (1984).
[5] J. Mader, S. Berko, H. Krakauer, and A. Bansil, Phys. Rev. Lett. **37**, 1232 (1976).
[6] M. Puska and R. Nieminen, Rev. Mod. Phys. **66**, 841 (1994).
[7] F. Kurp, M. Vos, Th. Tschentscher, A. S. Kheifets, J. R. Schneider, E. Weigold, and F. Bell, Phys. Rev. B **55**, 5440 (1997).
[8] W. Schülke, G. Stutz, F. Wohlert, and A. Kaprolat, Phys. Rev. B **54**, 12 381 (1996).
[9] S. Canney, M. Vos, A. S. Kheifets, N. Clisby, I. E. McCarthy, and E. Weigold, J. Phys.: Condens. Matter **9**, 1931 (1997).
[10] L. Lam and P. Platzman, Phys. Rev. B **9**, 5122 (1974).
[11] Y. Sakurai, Y. Tanaka, A. Bansil, S. Kaprzyk, A. T. Stewart, Y. Nagashima, T. Hyodo, S. Nanao, H. Kawata, and N. Shiotani, Phys. Rev. Lett. **74**, 2252 (1995).
[12] K. Hämäläinen, S. Manninen, C.-C. Kao, W. Caliebe, J. B. Hastings, A. Bansil, S. Kaprzyk, and P. M. Platzman, Phys. Rev. B **54**, 5453 (1996).
[13] E. Daniel and S. Vosko, Phys. Rev. **120**, 2041 (1960).
[14] F. Bell, T. Tschentscher, J. Schneider, and A. Rollason, J. Phys. B **24**, L533 (1991).
[15] P. Eisenberger and P. Platzman, Phys. Rev. A **2**, 415 (1970).
[16] P. Holm and R. Ribberfors, Phys. Rev. A **40**, 6251 (1989).
[17] T. Surić, Nucl. Instrum. Methods Phys. Res. A **314**, 240 (1992).
[18] B. Lundqvist and C. Lydén, Phys. Rev. B **4**, 3360 (1971).
[19] S. Berko, in *Positron Solid-State Physics,* Proceedings of the International School of Physics ''Enrico Fermi,'' Course LXXXIII, edited by W. Brandt and A. Dupasquier (North-Holland, Amsterdam, 1983).
[20] P. Suortti and T. Tschentscher, Rev. Sci. Instrum. **66**, 1798 (1995).
[21] T. Tschentscher, C. Metz, P. Suortti, A. Mauro, F. F. Kurp, T. Sattler, and F. Bell (unpublished).
[22] F. Kurp, A. E. Werner, J. R. Schneider, Th. Tschentscher, P. Suortti, and F. Bell, Nucl. Instrum. Methods Phys. Res. B **122**, 269 (1997).
[23] F. Fuggle, L. Watson, D. Fabian, and S. Affrossman, Surf. Sci. **49**, 61 (1975).
[24] S. Canney, M. Vos, A. S. Kheifets, X. Guo, I. E. McCarthy, and E. Weigold, Surf. Sci. **382**, 241 (1997).
[25] W. Assmann, P. Hartung, H. Huber, P. Staat, H. Steffens, and Ch. Steinhausen, Nucl. Instrum. Methods Phys. Res. B **85**, 726 (1994).
[26] H. Sakurai, F. Itoh, M. Ozaki, M. Ito, H. Kawata, and S. Kishimoto (unpublished).
[27] H. Skriver, *The LMTO Method* (Springer, Berlin, 1984).
[28] S. Y. Savrasov, Phys. Rev. B **54**, 16 470 (1996).
[29] S. Canney, A. Kheifets, M. Vos, and E. Weigold, J. Electron Spectrosc. Relat. Phenom. **88-91**, 247 (1998).
[30] F. Salvat, J. Martinez, R. Mayol, and J. Parellada, Comput. Phys. Commun. **42**, 93 (1986).
[31] S. Berko, M. Haghgooie, and J. Mader, Phys. Lett. **63A**, 335 (1977).
[32] P. Hayes, J. Williams, and J. Flexman, Phys. Rev. B **43**, 1928 (1991).
[33] M. Alatalo, B. Barbiellini, M. Hakala, H. Kauppinen, T. Korhonen, M. J. Puska, K. Saarinen, P. Hautojärvi, and R. M. Nieminen, Phys. Rev. B **54**, 2397 (1996).
[34] X Guo, S. Canney, A. S. Kheifets, M. Vos, Z. Fangand, S. Utteridge, I. E. McCarthy, and E. Weigold, Phys. Rev. B **54**, 17 942 (1996).
[35] S. Baber and R. Cousins, Nucl. Instrum. Methods **221**, 437 (1984).
[36] G. Bauer, Phys. Rev. B **27**, 5912 (1983).
[37] B. Lundqvist, Phys. Kondens. Mater. **7**, 117 (1968).
[38] B. Farid, V. Heine, G. Engel, and I. Robertson, Phys. Rev. B **48**, 11 602 (1993).
[39] L. Hedin, Phys. Rev. **139**, A796 (1965).
[40] K. Pandey and L. Lam, Phys. Lett. **43A**, 319 (1973).
[41] C. F. Bunge, J. Barrientos, and A. Bunge, At. Data Nucl. Data Tables **53**, 113 (1993).
[42] B. Holm and U. von Barth, Phys. Rev. B **57**, 2108 (1998).
[43] F. Aryasetiawan and O. Gunnarsson, Rep. Prog. Phys. **61**, 2337 (1998).
[44] D. Cardwell and M. Cooper, Philos. Mag. B **54**, 37 (1986).
[45] D. Cardwell and M. Cooper, J. Phys.: Condens. Matter **1**, 9357 (1989).
[46] N. Shiotani, N. Sakai, M. Ito, O. Mao, F. Itoh, H. Kawata, Y. Ameniya, and M. Ando, J. Phys.: Condens. Matter **1**, SA 27 (1989).
[47] L. Oberli, A. A. Manuel, R. Sachot, P. Descouts,and M. Peter, Phys. Rev. B **31**, 6104 (1985).
[48] C. Metz, Th. Tscheutscher, T. Sattler, K. Höppner, J. R. Schneider, K. Wittmauck, D. Frischke, and F. Bell (unpublished).
[49] U. von Barth and L. Hedin, J. Phys. C **5**, 1629 (1972).
[50] B. Králik, P. Delaney, and S. Louie, Phys. Rev. Lett. **80**, 4253 (1998).